Thermal ageing of a commercial LNT catalyst: Effects on the structure and functionalities

Thermal ageing of a commercial LNT catalyst: effects on the structure and functionalities.

Tommaso Pellegrinelli[1], Geoffrey McCullough[1], Roberto Caporali[2],

Iain Murray[2], Veronica Celorrio[3], Emma K Gibson[4], Christopher Hardacre[5], Alexandre Goguet[1,*]

[1]*Queen's University Belfast, Belfast, BT7 1NN, UK*
[2]*Ford Motor Company, Dunton Campus, Ford of Britain, Basildon, SS15 6EE, UK*
[3]*Diamond Light Source Ltd., Diamond House, Harwell Campus, Didcot, OX11 0DE, UK*
[4] *School of Chemistry, Joseph Black Building, University of Glasgow, Glasgow G12 8QQ, UK*
[5]*School of Chemical Engineering and Analytical Science, University of Manchester, Manchester, M13 9PL, UK*
*a.goguet@qub.ac.uk

Abstract

Hydrothermal degreening and ageing procedures were applied to a tri-metal (Pt-Pd-Rh) fully formulated lean NO_X Trap catalyst to evaluate the effects of thermal stress on the performances and structural properties. X-ray absorption fine structure (XAFS) analysis revealed that the average size of the platinum particles was the same after degreening and ageing treatments. The formation of a new phase of alloyed Pt-Pd was observed to increase with the thermal load. The size of the ceria particles also increased after the ageing treatment. NO_X storage capacity experiments revealed a substantial decrease of the concentration of active NO_X storage sites which correlated with both ageing and degreening protocols. The performances of the treated catalyst were evaluated through spatially resolved (SpaciMS) lean-rich cycles. During the lean phase, the impact of the decrease in storage sites was significant on the aged sample, where an enlargement of the area required to achieve full storage was observed. On the other hand, the regeneration functionalities did not appear to be particularly affected by ageing. Rather, the aged sample showed a decrease of oxygen storage capacity (OSC), which promoted a lower reductant consumption and therefore a quicker and more efficient reduction process. On the other hand, the different distributions of adsorbed species by the end of the lean phase produced greater spread presence of NH_3 and NO_X slip along the channels of the aged sample during the reduction.

1. Introduction

The Lean NO_X Trap (LNT) catalyst is one of the catalytic technologies adopted for NO_X emission control of the exhaust gases of passenger cars. Specifically, this catalytic system was designed to overcome the challenge of NO_X reduction to N_2 in oxidizing environments, which characterize lean-burn and diesel engines [1]. The LNT functioning relies on cyclical operations of NO_X storage and regeneration [2]. NO_X are first stored onto the catalyst during normal operations and, once the storage material reaches the target saturation, the catalyst is

regenerated. The regeneration occurs through a brief switch to a rich air-fuel ratio operated directly by the engine. As a consequence, a rich pulse of unburned fuel, CO and H_2 is sent to the exhaust and arrives at the catalyst downstream where it reduces the stored NO_X to N_2. However, the reduction of the adsorbed NO_X can lead to minor amounts of incomplete reduction products such as N_2O as well as to the full reduction product NH_3 [3–6].

Traditionally, the LNT systems were composed of a cordierite monolith coated with a high surface area support (Al_2O_3) with additional deposition of an alkaline or alkaline-earth metal (Ba or K), which is capable of storing NO_X in the form of nitrites or nitrates. Platinum was also added to the formulation as the active phase in the operations of NO_X storage and its subsequent reduction to N_2. This formulation has been progressively improved, with the addition of components to improve the durability of the catalyst and, also, to meet the increasingly stringent NO_X emission regulations. For example, ceria (CeO_2) was implemented to improve the catalyst low-temperature performance [7] and sulfur tolerance [8]. Eventually, multi-metallic compositions (Pt-Pd-Rh) were adopted in order to increase the thermal stability and selectivity towards N_2 [9–14].

Despite all these advances, the degradation of the catalyst remains of significant interest to automotive manufacturers. Vehicle-based studies of LNT ageing identified sulfur poisoning and platinum sintering as the main causes of deactivation [15–17]. It was found that SO_2 present in the exhaust gas could form $BaSO_4$, which prevents the barium from storing NO_x. In order to remove the sulfur from the barium phase, periodical de-sulfuration cycles are carried out by the engine management. Barium sulphate is a particularly stable compound, and temperatures above 600°C are required for its decomposition [18,19]. These types of conditions are particularly detrimental to the platinum particles, which tend to sinter at high temperatures, especially in the presence of oxygen [20,21]. Studies have been conducted on hydrothermally aged samples to decouple the effects of thermal degradation from sulfur poisoning [22,23]. For instance, Kim et al. [23] found a correlation between the growth of Pt crystallites and the decrease of NO_X storage performance. The authors also pointed out that the effects of ageing on Pt were less significant in the presence of a rich gas mixture, in agreement with previously reported findings. From a mechanistic perspective, platinum was found to have several roles in the storage process. Firstly, the metal is responsible for the oxidation of NO to NO_2, which is a necessary step in order to form barium nitrites and nitrates [24]. Secondly, the Pt/Ba perimetral interface is considered to be a crucial factor for an efficient NO_X storage process [25–27]. Indeed, Clayton et al. [28] demonstrated that improving the dispersion of Pt sites significantly enhanced the NO_X Storage Capacity (NSC) and NO_X Storage rate. In contrast, a substantial decrease in NSC, coupled with an increase in NH_3 selectivity, was observed as a consequence of Pt particle growth.

To date, spatially resolved techniques have been successfully adopted in the investigation of the properties of LNT systems [3,4,29–32]. Given the intrinsic integral nature of the catalyst, useful information can be obtained from the observation of species along the monolith channels. In particular, Choi et al. [4] showed that the sulfation process of the LNT proceeded axially along the catalyst, producing a displacement of the NO_X storage area, and an increase in NH_3 production towards the outlet of the catalyst. Spatially-resolved measurement techniques were also used by Easterling et al. to study the effect of hydrothermal treatments on the production of NH_3 in coupled LNT-SCR systems [33–35]. The study showed that Pt/Ba segregation produced a stretch of the NO_X storage zone during the lean phase, because a lower concentration of active storage sites was present.

In the present study, we combined X-ray absorption analysis (XAS) characterizations with spatially resolved capillary inlet mass spectrometers (Spaci-MS) techniques to describe the effect of thermal stress on the properties and performances of a commercial tri-metal LNT system. In particular, the effects of a mild and a severe hydrothermal treatment on the morphology were investigated and correlated with the NO_X storage and reduction functionalities.

2. Experimental

2.1.Samples and ageing protocols

Three fully formulated LNT cordierite monolith catalysts were supplied by Ford Motor Company. The main components of the washcoat were ceria, alumina, magnesium oxide, and barium oxide. A mixture of PGMs including platinum, palladium, and rhodium was deposited on the washcoat. One of the monoliths was left untreated as reference (indicated as Fresh or F sample), while the others two underwent hydrothermal ageing treatments. The first of these was treated for one hour at 650°C in air in the presence of water vapour. This sample was representative of the degreened state (D). The second sample, referred to as the aged sample (A), was treated at 800°C for 16 hours using the same hydrothermal conditions.

2.2. Catalyst Characterization

X-ray absorption spectroscopy (XAS). Measurements were performed on the B18 beamline at Diamond Light Source, operating with a ring energy of 3 GeV and at a current of 300 mA [36]. Calibration of the monochromator was conducted using the respective metal foils prior to the measurements. Pellets of the different samples were collected in transmission and fluorescence modes at the Rh K-edge (23219 eV), Pd K-edge (24350 eV) and Pt L3-edge

(11564 eV) simultaneously with the foils. The data was analysed using Athena and Artemis programs, which implement the FEFF6 and IFEFFIT codes [37].

X-ray photoelectron spectroscopy (XPS). Analysis was performed using a Kratos Axis SUPRA XPS fitted with a monochromated Al K_α X-ray source (1486.7 eV), a spherical sector analyser and 3 multichannel resistive plate, 128 channel delay line detectors. All data was recorded at 150W and a spot size of 700 x 300 μm. Survey scans were recorded at a pass energy of 160 eV, and high-resolution scans recorded at a pass energy of 20 eV. Electronic charge neutralization was achieved using an electron flood gun. Filament current = 0.27 A, charge balance = 3.3 V, filament bias = 3.8 V. All sample data was recorded at a pressure below 10^{-8} Torr and a room temperature of 294 K. Data was analysed using CasaXPS v2.3.19PR1.0. Peaks were fit with a Shirley background prior to component analysis. Lineshapes of LA (1.53,243) were used to fit components.

X-ray powder diffraction (XRD). The analyses were carried out on a Panalytical X'Pert diffractometer. Powder samples were subject to Cu Ka radiation operating at 40 kV and 40 mA. All analysis were carried out in continuous scan mode from 15 to 90° of 2teta with step size of 0.02°.

BET. The surface area was determined by BET analysis at -197°C with liquid nitrogen using a Micromeritics Tristar 3020 instrument.

2.3. SpaciMS experiments

Reactor Setup. The spatiotemporal analysis of the samples was performed with a spatially resolved capillary inlet mass spectrometer (SpaciMS). Further details of the equipment can be found elsewhere [38]. Typically, cores of 17 mm in diameter and 30 mm long were extracted from the central part of the monolith, wrapped in insulating tape, and placed in the reactor. The gas sampling was performed using an open-ended fused silica capillary with an outer diameter of 220 μm. A type K thermocouple with a diameter of 250 μm was used for temperature recording. The capillary and the thermocouple were placed in adjacent central channels of the monolith. Axial translation of the capillary and thermocouple was obtained via a z-motion linear stage which was controlled by a Thorlab APT Microstepping Controller (BSC101). Data regarding the speciation of the gas phase were collected through a Hiden HPR20 quadrupole mass spectrometer. The gas mixture was supplied through a series of gas mass flow controllers (Brooks 4800 Series). The total flow rate was 4.54 L min^{-1} for each experimental procedure. The oscillation between lean and rich conditions was operated by the 2 way VICI valve, controlled by an automated MATLAB program.

NO_X Storage Experiments. The total NO_x storage capacity (NSC) was evaluated for each sample at a temperature of 300 °C. To this aim, after a 30-minute pre-treatment with 0.4% hydrogen in argon at 300 °C, the probe was positioned at a downstream axial position of 9 mm from the monolith's front face, and the catalyst was exposed to a lean mixture containing 400 ppm of NO and 5% oxygen. These conditions were maintained until the concentration of the NO_X at the outlet matched the NO inlet concentration, a condition which implied that the catalyst surface was saturated with NO_X. The NSC of each catalyst was evaluated according to

$$NSC\ [ppm\ s\ mm^{-1}] = \frac{\int_0^t (C_{NOx}^{0mm}(t) - C_{NOx}^{9mm}(t))dt}{d} \qquad \text{Eqn 1.}$$

where d is the distance of the capillary from the front face of the catalyst, and C_{NOx} the concentration of NO_X in ppm.

Lean and Rich Cycling Experiments. The experimental procedure involved of a 30-min pre-treatment with 0.4% hydrogen in argon at 300 °C, followed by a series of 50 lean-rich cycles at the same temperature, lasting 120 and 60 s, respectively.

During the lean phase, the feed was composed of 400 ppm of NO and 5% O_2 with argon as a balance. During the rich phase and the pre-treatment, the inlet gas stream contained hydrogen at a concentration of 4000 ppm, helium as tracer, and a balance of argon. The same experimental procedure was repeated at various spatial positions of the catalyst in order to provide spatially resolved data.

Firstly, the probe was positioned before the inlet face of the monolith to evaluate the concentrations of the reactant species in the feed. Then, the same procedure was repeated after positioning the probe at different axial positions along the catalyst. The data was recorded at intervals of one millimetre over the first 9 mm of the fresh and de-greened samples, and the first 12 mm for the aged sample. The length of catalyst covered by the analysis was based on the length required to achieve total NO_X storage.

In order to maximize the signal to noise ratio, an averaging procedure was adopted. For each position and time, the signals of the species from each of Lean-Rich cycles were combined according to

$$x_i^{avg}(t,d) = \frac{\sum_{n=1}^{ntot} x_i^n(t,d)}{ntot} \qquad \text{Eqn 2.}$$

where $x_i^n(t,d)$ is the raw signal for the i-species at the n-cycle at the time t and position d, $ntot$ is the number of cycles averaged and x_i^{avg} is the averaged signal obtained.

For each series of 50 lean-rich cycles carried out at each spatial position, the first two cycles were discarded to ensure that the system had reached a stable and repeatable response between the lean and rich states. The remaining 48 cycles were combined in a single averaged cycle.

The gas species analysed, and their associated mass to charge ratio (m/z), were H2 (m/z = 2), He (m/z = 4), NH3 (m/z = 16-17), H2O (m/z = 18), N2 (m/z = 28), NOx (m/z = 30), Ar (m/z = 36), N2O (m/z = 46). The concentration of the gases was derived from the mass spectrometer signals through calibration carried out on the different reactants and products present in the reaction system. The results were compiled in the form of three-dimensional graphs (time, axial position, concentration) from which, in some cases, two-dimensional specific analyses were extracted when relevant.

The local integral amounts of each species, M_i^d $[ppm\ s]$, were evaluated for every axial position according to

$$M_i^d\ [ppm\ s] = \int_{t_0}^{t_1} C_i^d(t)dt \qquad \text{Eqn 3.}$$

where C_i^d [ppm] is the concentration of the i-species at the axial position d, and t_0-t_1 is the 0-120 s interval for the lean phase and 120-180 s the interval for the rich phase.

The quantities of interest estimated were the local NO_X Stored Amount (NSA), defined by

$$NSA^d[ppm\ s\ ] = \int_{0\ s}^{120\ s} (C_{NOx}^d(t) - C_{NOx}^{d-1}(t))dt \qquad \text{Eqn 4.}$$

and the cumulative hydrogen conversion, X_{H2}^d, given by

$$X_{H2}^d[\%] = \frac{M_{H2}^0 - M_{H2}^d}{M_{H2}^0} \qquad \text{Eqn 5.}$$

where M_{H2}^0 is the integral amount oh hydrogen recorded in the feed and M_{H2}^d the amount of hydrogen recorded at the axial position d.

3. Results and discussion

3.1. Characterization analysis

Table 1 reports the results of the BET analysis of the catalysts tested. It is worth mentioning that the characterizations were carried out on the washcoat of the catalytic brick after it was removed from the cordierite support. The surface area after the degreening treatment was slightly lower compared to the fresh sample which meant that the degreening treatment did not affect significantly the catalyst supports (Al_2O_3 and CeO_2). After the ageing treatment, a more severe degradation of the surface area was observed with a decrease of about 20% with respect to the fresh sample.

Table 1 Results of total NO_X storage capacity experiments. The evaluation was carried out 9 mm within the catalytic bed. Experiments were carried out until saturation of the surface was reached.

Catalyst	S_{BET} [m^2 g_{cat}^{-1}]	CeO_2 average size [nm]
Fresh	113	8.6
Degreened	111	8.7
Aged	92	12.9

Similar findings were observed with the XRD analysis as displayed in Figure 1. While the fresh and degreened samples showed broad and low intensity peaks related to CeO2, after ageing the same peaks appear more intense and sharper. This indicated a growth of the ceria particles with increased crystallinity [39]. Ceria average particle sizes were evaluated through Debye Sherrer equation and reported in Table 1.

Table 2 Surface atomic concentrations and ratios estimated by X-ray photoelectron spectroscopy (XPS).

	%Atomic concentration (%)				Atomic ratio
	Al	Ce	Mg	Ba	Ba/(Al+Ce+Mg)
Fresh	58.24	4.67	6.26	1.26	0.0182
Degreened	56.07	4.94	6.17	1.43	0.0213
Aged	61.95	3.96	6.48	1.48	0.0204

Table 2 summarizes XPS analysis that were performed on the samples. In accordance with the XRD analysis, alumina is not influenced by the thermal stress. At the same time, a decrease of the atomic concentration of the ceria was observed, in line with previously reported data.

Furthermore, thermal ageing appears to have a slightly positive effect on the barium atomic concentration ratio.

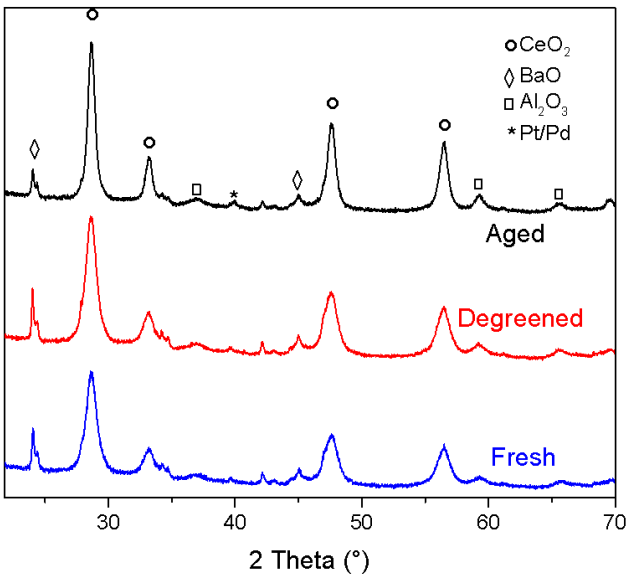

Figure 1 XRD profiles of fresh, degreened and aged samples.

Figure 2 reports a comparison of the EXAFS Fourier Transforms (FTs) of the fresh, degreened and aged samples at the Rh K-edge (A), Pd K-edge (B) and Pt L_{III}-edge (C). The Fourier Transform of the EXAFS data at the Rh K-edge were dominated by the Rh-O contribution (peak at ~1.6 Å, in Figure 3 (A)), and no significant change was observed with the ageing treatments (Tables 3-5). The possibility of rhodium particles encapsulation into the alumina support was also investigated [40]. However, no significant shift of the Rh K-edge in the XANES region was observed, nor clear evidence of Rh-Al contribution could be fitted to the EXAFS data. From the data measured at the Pd K-edge (Figure 2B), a slight increase of the alloying between Pd and Pd was observed. The degreened sample having a coordination to Pt of 2±1, which increases to 3.6 ± 0.9 after ageing. (Tables 3 to 5). In the case of the Pt L_{III}-edge, as shown in Figure 2C, an increase in coordination number to Pt atoms at a distance of 2.75Å, consistent with Pt metal, was observed on degreening (Tables 3 and 4). This likely indicates an increase in Pt NP size. The duration and temperature of treatment did not seem to have an effect on particle size, since similar Pt-Pt coordination numbers were observed for the degreened and aged samples (Tables 4 and 5). No change in Pt-O coordination was observed between the degreened and aged samples. In agreement with our observations, an early study by Morlang et al[12] described hydrothermally aged Pt-Pd model catalysts as alloyed Pt-Pd bimetallic structures proximal to PdO clusters. This type of structure was proved to limit the sintering of the platinum, preserving the catalytic properties. Apparently, the formation of Pt-Pd alloy prevents the formation of the volatile PtO_2 at high temperatures, which is responsible

of particle growth through Oswald ripening [11,13,21,41–43]. A linear combination analysis of the XANES of the Pd and Pt for the three ageing treatment was also performed. The results are reported in tables S1 and S2 and Figures S1 and S2 For both Pt and Pd a slight reduction of the metals can be observed from fresh to degreened to aged samples consistent with the formation of the Pd-Pt alloy phase. The linear combination analysis did not show any increase in the PtO2 content from the degreened to aged sample which might indicate that the alloying limited further formation of PtO2.

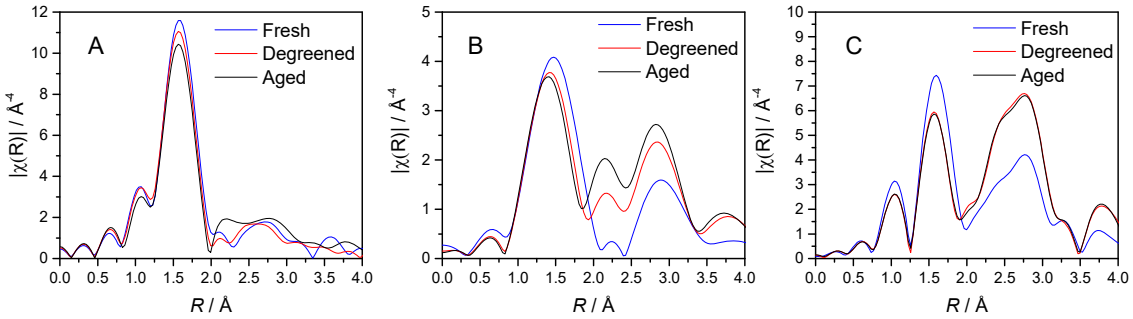

Figure 2 Magnitude component of the of the k^3 weighted, non-phase corrected, Fourier Transform of the EXAFS data for the fresh (F), degreened (D) and aged (A) samples at the Rh K-edge (A), Pd K-edge (B) and Pt LIII-edge (C).

Table 3 EXAFS distances and fitting parameters for the fresh sample at the different edges. Fitting parameters Rh edge: S02 = 0.842; fit range 3.0 < k < 12.0, 1.0 < R < 2.0. Fitting parameters Pd edge: S02 = 0.8; fit range 3.3 < k < 8.8, 1.0 < R < 3.5. Fitting parameters Pt edge: S02 = 0.83; fit range 3.5 < k < 11.7, 1.0 < R < 3.5.

	Scattering	CN	R / Å	σ^2 x 10^3 / Å^2	ΔE_0 / eV	R_{factor}
Rh K-edge	Rh-O	5.2 ± 0.7	2.04 ± 0.02	1.5 ± 1.1	1.8 ± 1.6	0.009
Pd K-edge	Pd-O	3.1 ± 0.3	2.02 ± 0.02	3 (fixed)	3 ±3	0.01
	Pd-Pd^0	2 ± 1	2.93 ± 0.04	7 (fixed)		
	Pd-Pt	1 ± 1	2.69 ± 0.08	7 (fixed)		
Pt L_{III}-edge	Pt-O	3.5 ± 0.3	1.99 ± 0.02	3 (fixed)	-10 ± 2	0.03
	Pt-Pt^0	4 ± 1	2.78 ± 0.02	7 (fixed)		
	Pt-Pt^{PtO}	3 ± 2	3.08 ± 0.04	8 (fixed)		

Table 4 EXAFS distances and fitting parameters for the degreened sample at the different edges. Fitting parameters Rh edge: S02 = 0.842; fit range 3.0 < k < 12.0, 1.0 < R < 2.0. Fitting parameters Pd edge: S02 = 0.8; fit range 3.2 < k < 8.8, 1.0 < R < 3.5. Fitting parameters Pt edge: S02 = 0.83; fit range 3.5 < k < 11.7, 1.0 < R < 3.5.

	Scattering	CN	R / Å	σ^2 x 10^3 / Å^2	ΔE_0 / eV	R_{factor}

Rh K-edge	Rh-O	5.3 ± 0.7	2.03 ± 0.02	1.7 ± 1.6	1.9 ± 1.4	0.009
Pd K-edge	Pd-O	2.8 ± 0.2	2.01 ± 0.02	3 (fixed)	1 ± 2	0.007
	$Pd\text{-}Pd^{0}$	2.0 ± 0.7	2.90 ± 0.04	7 (fixed)		
	Pd-Pt	2 ± 1	2.79 ± 0.04	7 (fixed)		
Pt L_{III}-edge	Pt-O	2.7 ± 0.3	1.97 ± 0.01	3 (fixed)	-8 ± 2	0.02
	$Pt\text{-}Pt^{0}$	7.7 ± 0.9	2.77 ± 0.01	7 (fixed)		
	$Pt\text{-}Pt^{PtO}$	3 ± 1	3.06 ± 0.03	8 (fixed)		

Table 5 EXAFS distances and fitting parameters for aged sample at the different edges. Fitting parameters Rh edge: S02 = 0.842; fit range 3.0 < k < 12.0, 1.0 < R < 2.0. Fitting parameters Pd edge: S02 =0.8; fit range 3.3 < k < 8.8, 1.0 < R < 3.5. Fitting parameters Pt edge: S02 = 0.83; fit range 3.5 < k < 11.7, 1.0 < R < 3.5.

	Scattering	CN	R / Å	σ^2 x 10^3 / $Å^2$	ΔE_0 / eV	R_{factor}
Rh K-edge	Rh-O	4.8 ± 0.7	2.03 ± 0.02	1.7 ± 1.6	2.6 ± 2.0	0.010
Pd K-edge	Pd-O	2.7 ±0.2	2.00 ± 0.01	3 (fixed)	-0 ± 2	0.004
	$Pd\text{-}Pd^{0}$	2.0 ± 0.6	2.87 ± 0.03	7 (fixed)		
	Pd-Pt	3.6 ± 0.9	2.80 ± 0.02	7 (fixed)		
Pt L_{III}-edge	Pt-O	2.7 ± 0.2	1.97 ± 0.01	3 (fixed)	-8 ± 2	0.02
	$Pt\text{-}Pt^{0}$	7.9 ± 0.9	2.77 ± 0.01	7 (fixed)		
	$Pt\text{-}Pt^{PtO}$	3 ± 2	3.04 ± 0.03	8 (fixed)		

3.2. NO_x storage capacity tests

The results of the NO_x storage capacity (NSC) experiments are reported in Figure 3. From a comparison with the fresh sample, the amount of stored NO_x at steady state decreased by 27% upon the degreening treatment and 76% with the ageing treatment. The decrease of the NO_X storage capacity induced by thermal treatments is well reported in literature [15,23,44]. In particular, similar findings were reported by Ji et al. [44], who suggested that the lower NSC is a consequence of a decrease of Pt-Ba interface area, which reduces the number of active sites dedicated to NO_X storage. Indeed, mechanistic studies on Pt-Ba systems suggested that the proximity between the two components greatly enhances the transport of NO_x to the barium layer, which is considered the rate determining step [25–27]. This hypothesis is supported by the work of Clayton et al. [28], who demonstrated a positive correlation between the NSC and the dispersion of platinum particles.

In our case, XAFS analysis revealed that platinum particle size was increasing upon hydrothermal treatments. However, a discrepancy between Pt particle size and NSC loss was

observed. In fact, the degreened and aged samples reported similar average particle size, but also a significant difference in terms of NSC. Interestingly, the main difference between the degreened and the aged sample was a significant increase of the degree of Pd-Pt alloying. Previous studies have investigated the effect of Pt-Pd alloying on the NO oxidation rate of Pt particles[45]. The findings suggested that alloying between Pt and Pd does not affect significantly the NO oxidation mechanism. However, in the case of NO_X Storage, the role of Pt goes beyond the sole NO oxidation and influences directly the number of active sites. In fact, as demonstrated by Weiss et al[25], platinum particles are responsible for the formation and transport of the oxidant N_2O_4 to the nearby barium sites, which is required for the formation on nitrates. To the best of our knowledge, in the present results are the first suggesting a possible negative effect of the alloying on the NO_X storage mechanism.

Ultimately, another possible route for the decrease of active sites could be the degradation of storage materials. However, while a significant but not severe sintering was observed on ceria, XPS analysis revealed that barium surface atomic ratio did not display significant changes through hydrothermal treatments.

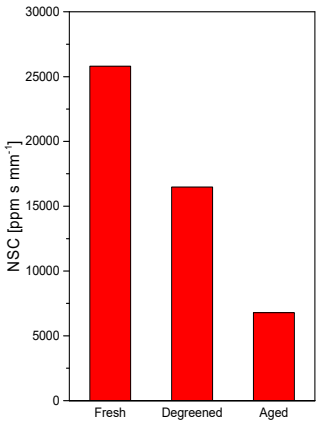

Figure 3 Results of total NO_X storage capacity experiments. The evaluation was carried out 9 mm within the catalytic bed. Experiments were carried out until saturation of t

3.3. Lean-Rich Cycles Experiments

Lean phase. Figure 4 reports the integral amount of NO_X during the lean phase at different axial position for the fresh (F), degreened (D) and aged (A) samples obtained during lean-rich cycles.

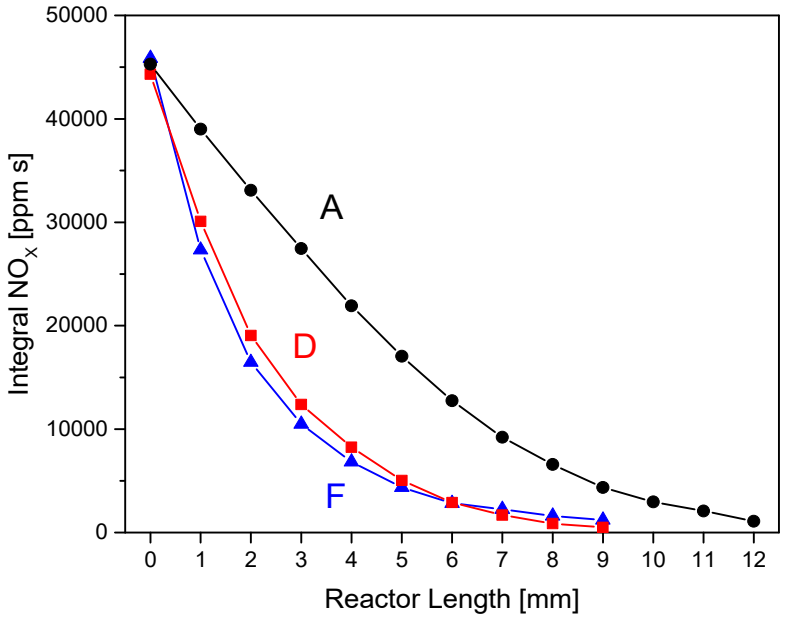

Figure 4 Integral amount of NO_X concentration recorded during the lean phase at different location of the samples: Fresh (F), degreened (D) and aged(A).

At each degree of ageing, the integral NO_X decreased along the catalytic channel as the NO_X got trapped by the storage material. However, the length required to achieve full storage over the full lean phase increased significantly after the ageing treatment. While the fresh and degreened samples stored the full amount of NO_X in the first 9 mm of the catalyst, the aged sample required 12 mm to reach full trapping. Similar findings were reported by Easterling et al [46], who explained an enlargement of the storage area as a consequence of the loss of active storage sites induced by ageing. These results are in agreement with the NO_X storage capacity experiments reported in Figure 3. However, it is worth noting that only a slight difference in the storage axial distribution was observed between the fresh and the degreened samples, even if the degreened sample displayed a 25% lower NO_X storage capacity.

A quantification of the amount of NO_X stored was carried out for each section (Figure 5) of the monoliths, which shows the limitations imposed by the decrease of NSC to the storage of equivalent amounts of NO_X. The amount of NO_X stored was extracted from the spatially resolved NO_X mass balances and represents the value obtained at the end of the lean phase.

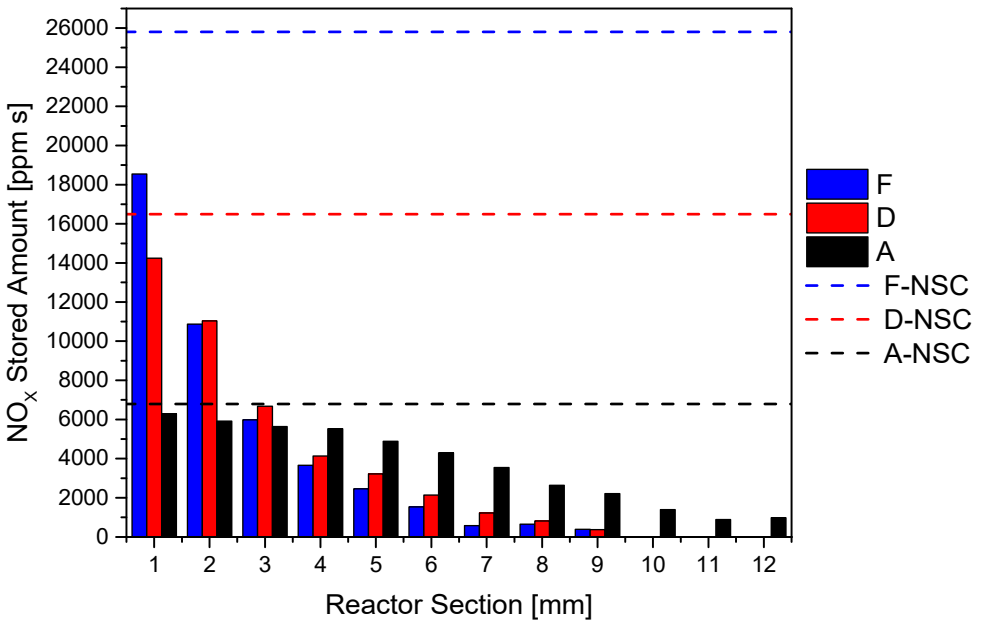

Figure 5 NO_X Stored Amount at each section of the catalysts: Fresh (F), Degreened (D) and Aged (A). The graph reports also the NO_X Storage Capacities as dash lines for each catalyst.

For the fresh sample, a comparison between the amount of NO_X stored and the NSC clearly showed that every section of the channel was far from reaching saturation of the sites. While the degreened sample showed a value that was proximal to its NSC in the 0-1 mm section. Indeed, the same section saw the highest difference in terms of stored amount between the fresh and the degreened samples. This difference was subsequently compensated by the degreened sample by filling in the sections downstream, where the amount of NO_X observed is slightly higher with respect to the fresh sample.

The aged sample, on the other hand, was affected with a dramatic decrease of the NSC. As a consequence, the limited number of sites produced a spread axial distribution of the NOx storage along the catalyst's channel. In this case, the amount of NO_X trapped in the 0-3 mm section of the reactor appeared to be approaching asymptotically the NSC value. These results suggest that the decrease of NSC was the main limiting factor for the aged sample, which was confirmed by the inflexion point located at the 5 mm section where the local amount of NO_X started to significantly differ from the NSC value. The decrease in the NSC is consecutive to the structural alterations due to the ageing treatments as described in the NSC study. These include Pt particles growth and alloying between Pt and Pd phases. Both degradation mechanisms were indicated as possible routes for a decrease of the concentration of active storage sites and, therefore, of the NSC value. Ceria phase also displayed sintering upon ageing treatment, although this feature was seen only on the aged sample.

Rich phase. After exposure to 120 s lean phase, the reactor feed was switched abruptly to a gas mixture containing H_2 at a concentration of 4000 ppm. The duration of the rich phase was 60 seconds and was chosen to ensure complete regeneration of the trap after each cycle. As described in previous studies [29,47,48] hydrogen is highly reactive at the chosen temperature, which makes the feed rate of the reductant the limiting factor in the overall NO_X reduction process.

An example of the temporal speciation during the rich phase is reported in Figure 6, the graph corresponds to the evolution of the species recorded at 5 mm within the channel of the aged sample. The first species observed, on switching to the rich phase, was the release of NO_X also known as NO_X 'puff', followed by the formation of nitrogen and ammonia. The hydrogen breakthrough occurred only at a time point corresponding to the beginning of the appearance of the ammonia peak, when most of the adsorbed species have already been converted. This sequence of species is consistent with the reduction front model [5,29,31,47], which ascribes the regeneration of the trap as a plug flow type movement, typical of systems that operate at feed-limited conditions. This time shift of the hydrogen front can be observed through the comparison between the hydrogen recorded before the inlet of the catalyst and the hydrogen observed at 5 mm. In fact, the delay displayed by the reductant after 5 mm is not due to the time required for the gas to flow through the channel, which is negligible (less than 0.01 s at 9 mm), but by the consumption of the frontal portion of the reductant.

Though the samples reported similar features, which meant that the regeneration mechanism was unchanged through the different types of ageing, significant variation of the total amount of species and transient on-set times were observed between samples.

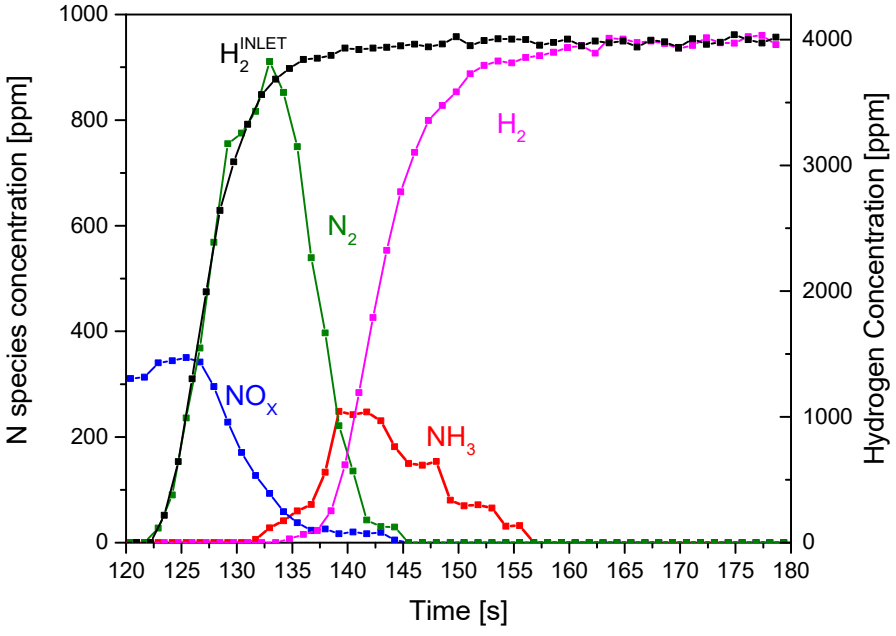

Figure 6 Example of temporal analysis of the gas species recorded during the rich phase. In particular, the graph reports the concentrations at 5 mm for the aged sample.

A comparison of the differences in terms of species concentrations and time scale between samples is reported in Figure 7. It displays the spatiotemporal analysis for the nitrogen, ammonia and hydrogen for the fresh degreened and aged samples. Only 9 out of the 12 mm of monolith measured for the aged sample are reported in the graph for comparison reasons. For each sample, in agreement with the previously explained Figure 6, the three species appeared in different spatiotemporal areas. Nitrogen was observed at the beginning of the regeneration, followed by the NH_3 and eventually by the H_2 front. The N_2 appeared at the location where it was formed and then was transported unreacted towards the outlet. Ammonia, after being locally generated, was capable of reacting downstream with the stored nitrates and form N_2, which explain its limited on-set time along the catalyst. The boundary between the nitrogen and hydrogen zones indicates the exposure time required for each section to achieve complete regeneration. At higher exposures times, as the regeneration of the catalyst progresses, the H_2 front progresses within the channel. At each position, the exposure time required to achieve regeneration of the fresh catalyst (Figure 7 left) appears to be longer compared to the degreened sample (Figure 7 centre), and significantly longer than for the aged sample (Figure 7 right). Therefore, different amounts of H_2 were consumed to achieve complete regeneration depending on the state of ageing of the catalyst. Consistently, the aged sample reported a significantly higher concentration of N_2 in the 6-9 mm axial location of the catalyst compared to the other samples, which meant that the N_2 formation rate was promoted by a higher H_2 availability.

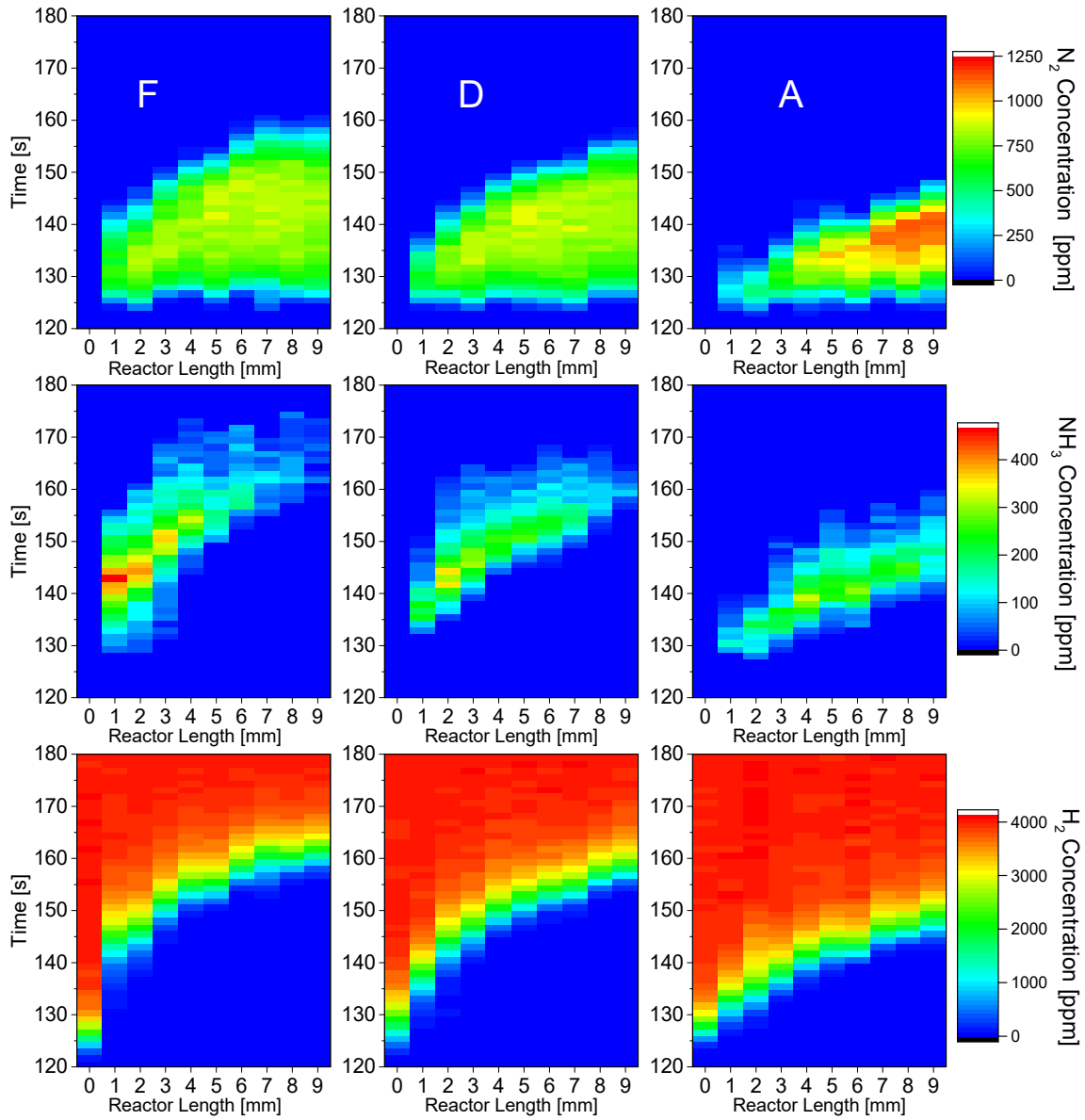

Figure 7 Nitrogen (top), ammonia (centre) and hydrogen (bottom) spatio-temporal analysis during the rich phase for fresh (F) degreened (D) and aged (A) samples.

The amount of hydrogen consumed by each sample was evaluated using integral conversions (Figure 8). As expected, the regeneration required different amounts of hydrogen depending on the ageing stage, with the consumption of hydrogen inversely proportional to the degree of ageing. Since similar global amounts of NO_X were stored on the samples, the difference in terms of hydrogen conversion must be associated with the PGMs and ceria[49]. Characterization analyses revealed that, following ageing treatments, an increase of size of Pt and CeO_2 particles occurred. Previous studies have identified a decrease in the oxygen storage capacity (OSC) in LNT systems related to sintering of platinum and ceria [44,46]. This aspect was described in great details by Gänzler et al. in an *in situ* time-resolved XAS study of Pt-CeO_2-Al_2O_3 catalysts [49]. In this investigation, they observed that lowering the dispersion of platinum particles produced a decrease of the reducibility of the CeO_2. According to the author,

this was due to the decrease of Pt-ceria interface, which hindered the reduction rate of the ceria. In the present case, the consequence of the Pt-ceria sintering was a smaller portion of the ceria being reduced during the rich phase. Consequently, comparing the fresh samples and the aged sample, the latter required less hydrogen for the reduction of the nitrates located on the barium phase.

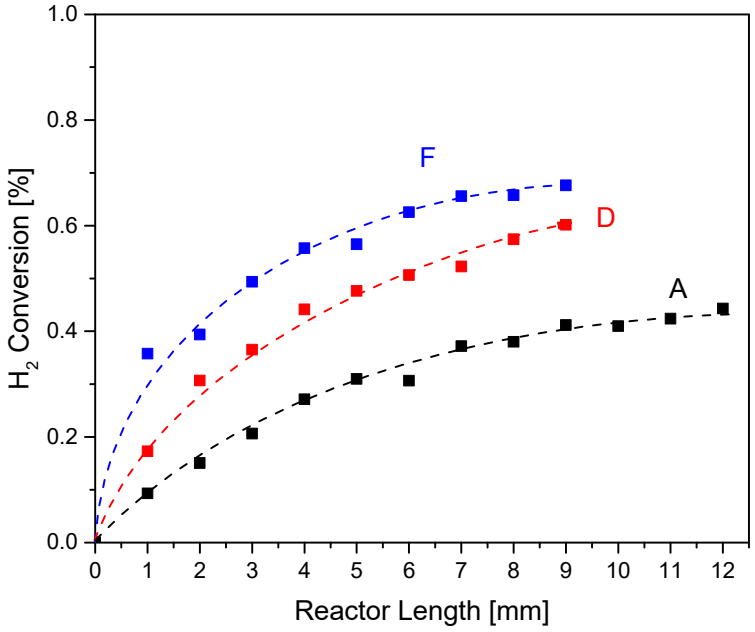

Figure 8 Hydrogen cumulative conversion at each section of the catalysts: Fresh (F), Degreened(D) and Aged(A). The dash lines are intended to guide the eye.

Figure 9 reports the integral amount of NO_X recorded during the rich phase as function of the axial position. This release of NO_X at the onset of the rich phase is known as a NO_x 'puff' and is associated with a reduction in the partial pressure of oxygen, and/or an increase in temperature that leads to the decomposition of part of the surface nitrates [2]. It was observed that the fresh and degreened samples showed similar behaviour, with a NO_x release upstream followed by gradual re-adsorption of the NO_X along the channel. Conversely, the aged sample displayed an increase of the amount of NO_X released up to 7 mm, after which point the NO_X began to decrease. The net increase of NO_X in the first section of the aged catalyst is likely the consequence of the high degree of saturation in the same section (Figure 5) which would strongly limit the possibility of re-adsorption. This feature has also been observed in the lean phase, during which the low NSC displayed by the aged sample produced a slower adsorption process. The links between the structural degradation and the NSC have been discussed in Section 3.2, where the sintering of platinum and the formation of a Pt-Pd alloy were indicated as the main causes for the loss of available storage sites observed on the sample after

hydrothermal treatment. However, other factors might be contributing to an increase of the NO_X spike, such as a less stable type of adsorbed species. Ultimately, the NO_X slip caused a displacement of NO_X from a high saturation zone at the inlet to the outlet of the catalyst, where more free sites are present. Therefore, a re-distribution of the adsorbed of NO_X occurred in the first instants of rich phase.

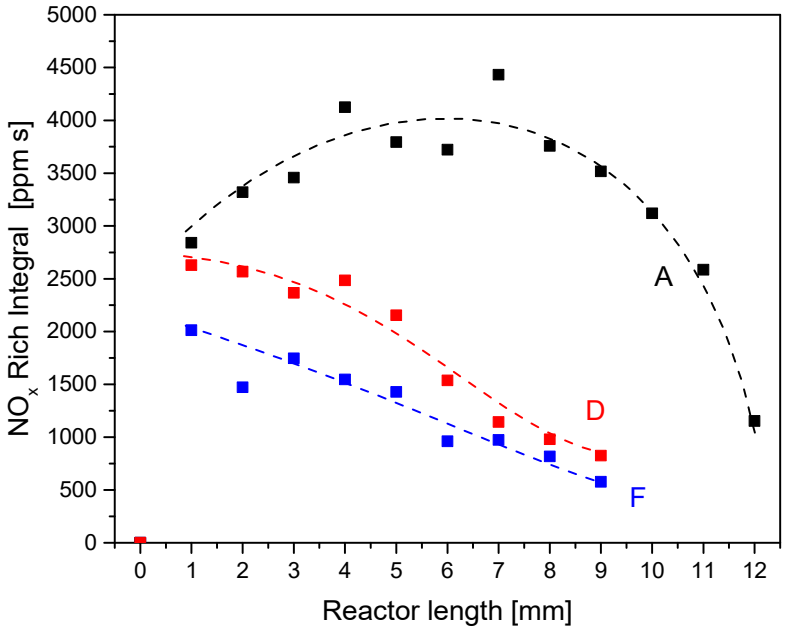

Figure 9 Integral NO_X amount observed during the rich phase at each section of the catalysts: Fresh (F), Degreened(D) and Aged(A). The dash lines are intended to guide the eye.

The integral amounts of N_2 are reported in Figure 10. Molecular nitrogen was the first reduced product observed during the regeneration of the trap (i.e. subsequent to the NO_X "puff") and, under these experimental conditions, the main reduction product for the catalysts. The main source of nitrogen is the reduction of surface nitrates, however, the reaction of NH_3 with stored nitrates and O_2 can give a substantial contribution. The fresh sample displayed the highest amount of nitrogen at all axial positions, in agreement with the distribution of the stored NO_X. As expected, the aged sample showed the lowest amount of nitrogen, however, the value at 12 mm was similar to the one displayed by the other samples. This meant that the formation of nitrogen, on the aged sample, was limited by the availability of stored NO_X and that the regeneration functionality of the catalyst was preserved through the hydrothermal ageing. This is consistent with the XAS results which did not show any significant alteration of the Rh upon the ageing treatments.

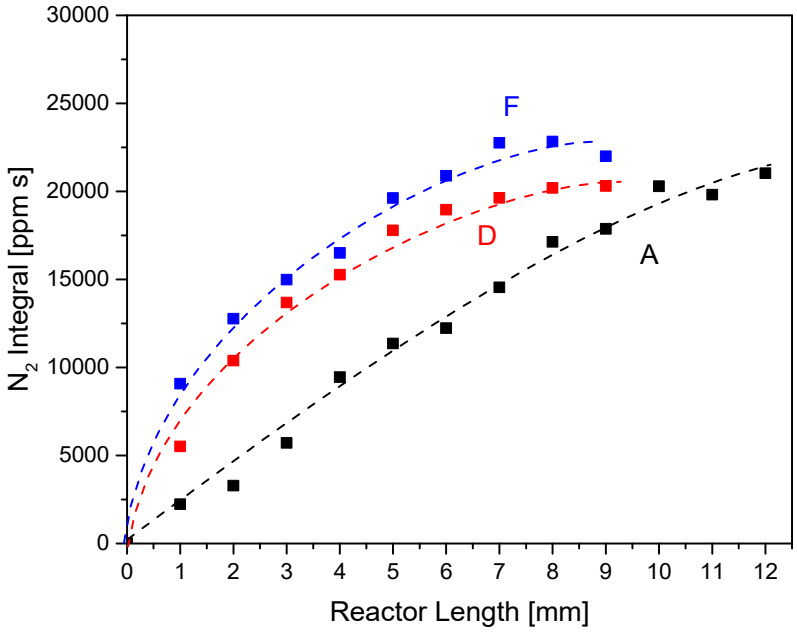

Figure 10 Integral N_2 amount observed during the rich phase at each section of the catalysts: Fresh (F), Degreened(D) and Aged(A). The dash lines are intended to guide the eye.

The last species observed before the appearance of the hydrogen breakthrough was NH_3. It is a well-known intermediate in a parallel route to the direct production of nitrogen during the regeneration of a NO_x Trap, which, if not fully oxidised can be found in the by-products [4,34,50,51]. According to the literature, the formation of ammonia is favoured by a local high H_2/NO_x ratio during the regeneration phase. Additionally, NH_3 was demonstrated to be highly reactive in the reduction of stored NO_X to N_2 [51]. In the present case, the presence of NH_3 was observed towards the end of the N_2 formation, when the majority of the adsorbed NO_X had already been converted. The remaining nitrates were then exposed to an abrupt increase of hydrogen concentration resulting in the formation of NH_3. In fact, for each sample, ammonia was observed to track the formation of nitrogen, just before the hydrogen breakthrough (Figure 7).

The spatially resolved NH_3 integral concentration is reported in Figure 11. For the fresh sample, the maximum ammonia selectivity was observed in the proximity of the inlet. Moving towards the back of the catalyst, the rate of ammonia consumption prevailed, and the overall amount dropped progressively along the catalyst. Eventually, only traces of NH_3 were found at 9 mm.

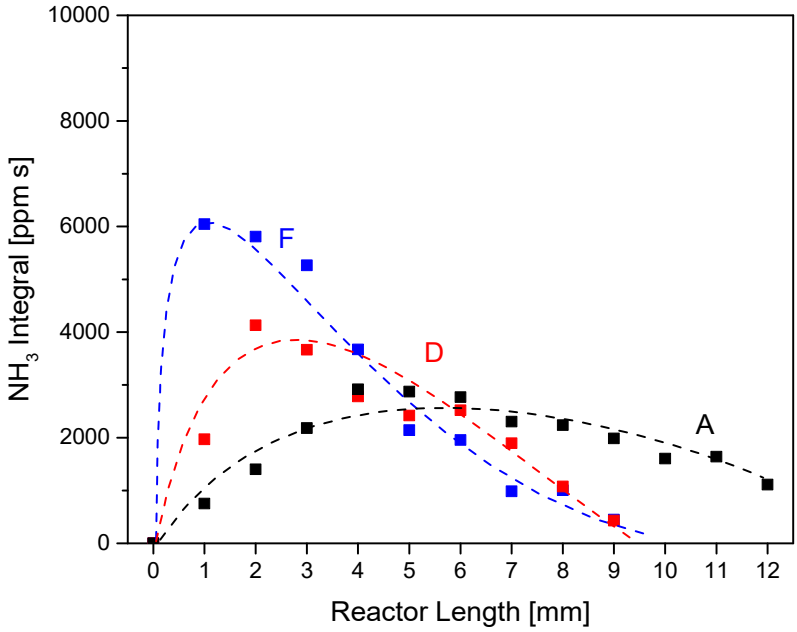

Figure 11 Integral NH_3 amount observed during the rich phase at each section of the catalysts: Fresh (F), Degreened(D) and Aged(A). The dash lines are intended to guide the eye.

Interestingly, for the degreened sample the integral ammonia selectivity peaked at 2 mm and the amount of ammonia was lower with respect to the fresh sample. The aged sample displayed a peak in ammonia selectivity at 4 mm, with a slower increase compared to the other two samples. Moreover, the consumption of ammonia was significantly slower downstream. Partridge et al[29] refer to the area where ammonia increases as a build-up zone, and underlines that this area covers the high-NO_X-density section of the catalyst, where around 50% of NO_X are stored. In agreement with this hypothesis, the spread distribution of stored NO_X in the case the aged sample produced a longer NH_3 build-up zone compared with the fresh and degreened samples which saw the majority of the NOx was stored in the first 3 mm (Figure 5).

4. Conclusions

In the present study, we reported the effect of hydrothermal treatments on the morphology and lean-rich functionalities of a commercial LNT catalyst. Characterization analysis revealed that ceria and platinum were the most affected components of the catalyst. In particular, a significant sintering of ceria associated with decrease of surface area was observed upon ageing. Platinum particles presented a substantial growth; however, the final particle size appears to be similar between the degreened and the aged sample. Conversely, the alloying of Pt-Pd increased at each ageing step.

The effect of the catalyst degradation was evident from performance studies where a decrease of active sites for NO_X storage and O_2 storage was evident. The amount of active sites for NO_X storage was evaluated through NO_X Storage Capacity experiments, and decreases of number of sites were observed after degreening treatment (-27% NSC), and ageing treatment (-76% NSC).

During the lean phase of lean-rich cycles, the lack of active storage sites produced a 33% stretch of the storage area on the aged sample. Indeed, by the end of the lean phase, the front part of the catalyst was approaching saturation of sites. While the NO_X storage performance of the degreened sample was unchanged with respect to the fresh sample.

During the rich phase, the combination of the lack of oxygen stored and a spread distribution of NO_X promoted a fast development of the H_2 front within the aged sample. In fact, less H_2 was consumed during its regeneration and the local concentration of N_2 was higher. Ultimately, the NH_3 formation and consumption to N_2 was observed occurring locally during the regeneration of the catalyst concomitantly with the progression of the H_2 front. The amount of NH_3 detected along the catalyst varied with ageing and subsequent impact on its formation/consumption rates. The consumption of NH_3 appeared to be impaired upon ageing, leading to a more distributed presence of ammonia.

Acknowledgements

The work reported was supported by Ford Motor Company. The authors wish to acknowledge the Diamond Light Source for provision of beamtime (SP15151). The x-ray photoelectron (XPS) data collection was performed at the EPSRC National Facility for XPS (“HarwellXPS”), operated by Cardiff University and UCL, under Contract No. PR16195.

References

[1] N. Takahashi, H. Shinjoh, T. Iijima, T. Suzuki, K. Yamazaki, K. Yokota, H. Suzuki, N. Miyoshi, S. Matsumoto, T. Tanizawa, T. Tanaka, S. Tateishi, K. Kasahara, The new concept 3-way catalyst for automotive lean-burn engine: NOx storage and reduction catalyst, Catal. Today. 27 (1996) 63–69. https://doi.org/10.1016/0920-5861(95)00173-5.

[2] W.S. Epling, L.E. Campbell, A. Yezerets, N.W. Currier, J.E. Parks, Overview of the Fundamental Reactions and Degradation Mechanisms of NOx Storage/Reduction Catalysts, Catal. Rev. 46 (2004) 163–245. https://doi.org/10.1081/CR-200031932.

[3] D. Mráček, P. Kočí, M. Marek, J.S. Choi, J.A. Pihl, W.P. Partridge, Dynamics of N2 and N2O peaks during and after the regeneration of lean NOx trap, Appl. Catal. B

Environ. 166–167 (2015) 509–517. https://doi.org/10.1016/j.apcatb.2014.12.002.

[4] J.-S. Choi, W.P. Partridge, J.A. Pihl, M.-Y. Kim, P. Kočí, C.S. Daw, Spatiotemporal distribution of NOx storage and impact on NH3 and N2O selectivities during lean/rich cycling of a Ba-based lean NOx trap catalyst, Catal. Today. 184 (2012) 20–26. https://doi.org/10.1016/j.cattod.2011.11.007.

[5] Š. Bártová, P. Kočí, D. Mráček, M. Marek, J.A. Pihl, J.-S. Choi, T.J. Toops, W.P. Partridge, New insights on N2O formation pathways during lean/rich cycling of a commercial lean NOx trap catalyst, Catal. Today. 231 (2014) 145–154. https://doi.org/10.1016/j.cattod.2013.11.050.

[6] N.K. Margaritis, O.A. Haralampous, G.C. Koltsakis, Modeling of the NO x trap and experimental validation using ultra-fast NO x analyzers, Top. Catal. 42–43 (2007) 65–69. https://doi.org/10.1007/s11244-007-0153-7.

[7] Z. Zhou, M.P. Harold, D. Luss, Comparison of Pt-BaO/Al2O3 and Pt-CeO2/Al2O3 for NOx storage and reduction: Impact of cycling frequency, Appl. Catal. B Environ. (2019). https://doi.org/10.1016/j.apcatb.2019.05.044.

[8] V. Easterling, Y. Ji, M. Crocker, J. Ura, J.R. Theis, R.W. McCabe, Effect of ceria on the desulfation characteristics of model lean NO x trap catalysts, Catal. Today. 151 (2010) 338–346. https://doi.org/10.1016/j.cattod.2009.12.007.

[9] J.R. González-Velasco, J.A. Botas, R. Ferret, M. Pilar González-Marcos, J.-L. Marc, M.A. Gutiérrez-Ortiz, Thermal aging of Pd/Pt/Rh automotive catalysts under a cycled oxidizing–reducing environment, Catal. Today. 59 (2000) 395–402. https://doi.org/10.1016/S0920-5861(00)00304-7.

[10] J.. U. Theis J.; McCabe, R., The Effects of Platinum and Rhodium on the Functional Properties of a Lean NOx Trap, SAE Tech. Pap. Ser. 01 (2007). https://doi.org/10.4271/2007-01-1055.

[11] C. Carrillo, T.R. Johns, H. Xiong, A. Delariva, S.R. Challa, R.S. Goeke, K. Artyushkova, W. Li, C.H. Kim, A.K. Datye, Trapping of mobile Pt species by PdO nanoparticles under oxidizing conditions, J. Phys. Chem. Lett. 5 (2014) 2089–2093. https://doi.org/10.1021/jz5009483.

[12] A. Morlang, U. Neuhausen, K. V. Klementiev, F.W. Schütze, G. Miehe, H. Fuess, E.S. Lox, Bimetallic Pt/Pd diesel oxidation catalysts: Structural characterisation and catalytic behaviour, Appl. Catal. B Environ. 60 (2005) 191–199. https://doi.org/10.1016/j.apcatb.2005.03.007.

[13] C. Carrillo, A. DeLaRiva, H. Xiong, E.J. Peterson, M.N. Spilde, D. Kunwar, R.S. Goeke, M. Wiebenga, S.H. Oh, G. Qi, S.R. Challa, A.K. Datye, Regenerative trapping: How Pd improves the durability of Pt diesel oxidation catalysts, Appl. Catal. B Environ. (2017). https://doi.org/10.1016/j.apcatb.2017.06.085.

[14] Y. Ren, M.P. Harold, NO x storage and reduction with H2 on Pt/Rh/BaO/CeO2: Effects of Rh and CeO2 in the absence and presence of CO2 and H2O, ACS Catal. 1 (2011) 969–988. https://doi.org/10.1021/cs200252r.

[15] S. Benramdhane, C.N. Millet, E. Jeudy, J. Lavy, V.B. Aubé, M. Daturi, Impact of thermal and vehicle aging on the structure and functionalities of a lean NOx-trap, Catal. Today. 176 (2011) 56–62. https://doi.org/10.1016/j.cattod.2011.03.049.

[16] J. Wang, Y. Ji, G. Jacobs, S. Jones, D.J. Kim, M. Crocker, Effect of aging on NOx reduction in coupled LNT-SCR systems, Appl. Catal. B Environ. 148–149 (2014) 51–61. https://doi.org/10.1016/j.apcatb.2013.10.037.

[17] J. De Abreu Goes, A. Kristoffersson, T. Wentworth, L. Olsson, Detailed Characterization Studies of Vehicle and Rapid Aged Commercial Lean NOx Trap Catalysts, Ind. Eng. Chem. Res. (2018). https://doi.org/10.1021/acs.iecr.8b01468.

[18] J.E.D.A. Goes, A. Kristoffersson, L. Olsson, Sulfur poisoning effects on modern lean nox trap catalysts components, Catalysts. 9 (2019) 1–18. https://doi.org/10.3390/catal9060492.

[19] F. Rohr, S.D. Peter, E. Lox, M. Kögel, A. Sassi, L. Juste, C. Rigaudeau, G. Belot, P. Gélin, M. Primet, On the mechanism of sulphur poisoning and regeneration of a commercial gasoline NOx-storage catalyst, Appl. Catal. B Environ. 56 (2005) 201–212. https://doi.org/10.1016/j.apcatb.2004.09.011.

[20] E. Solano, J. Dendooven, R.K. Ramachandran, K. Van De Kerckhove, T. Dobbelaere, D. Hermida-Merino, C. Detavernier, Key role of surface oxidation and reduction processes in the coarsening of Pt nanoparticles, Nanoscale. 9 (2017) 13159–13170. https://doi.org/10.1039/c7nr04278g.

[21] T.W. Hansen, A.T. Delariva, S.R. Challa, A.K. Datye, Sintering of catalytic nanoparticles: Particle migration or ostwald ripening?, Acc. Chem. Res. 46 (2013) 1720–1730. https://doi.org/10.1021/ar3002427.

[22] D. Heui Kim, Y.-H. Chin, G. G. Muntean, A. Yezeretz, N. W. Currier, W. S. Epling, H.-Y. Chen, H. Hess, C. H. F. Peden, Relationship of Pt Particle Size to the NOx Storage Performance of Thermally Aged Pt/BaO/Al2O3 Lean NOx Trap Catalysts, Ind. &

Eng. Chem. Res. 45 (2006) 8815–8821. https://doi.org/10.1021/ie060736q.

[23] D.H. Kim, Y. Chin, G.G. Muntean, A. Yezeretz, N.W. Currier, W.S. Epling, H. Chen, H. Hess, C.H.F. Peden, Relationship of Pt Particle Size to the NO x Storage Performance of Thermally Aged Pt / BaO / Al 2 O 3 Lean NO x Trap Catalysts, (2006) 8815–8821. https://doi.org/10.1021/ie060736q.

[24] S.S. Mulla, N. Chen, L. Cumaranatunge, G.E. Blau, D.Y. Zemlyanov, W.N. Delgass, W.S. Epling, F.H. Ribeiro, Reaction of NO and O2 to NO2 on Pt: Kinetics and catalyst deactivation, J. Catal. 241 (2006) 389–399. https://doi.org/10.1016/j.jcat.2006.05.016.

[25] B.M. Weiss, K.B. Caldwell, E. Iglesia, NO $_x$ Interactions with Dispersed BaO: Adsorption Kinetics, Chemisorbed Species, and Effects of Oxidation Catalyst Sites, J. Phys. Chem. C. 115 (2011) 6561–6570. https://doi.org/10.1021/jp110604j.

[26] S.S. Chaugule, A. Yezerets, N.W. Currier, F.H. Ribeiro, W.N. Delgass, “Fast” NOx storage on Pt/BaO/Al2O3 Lean NOx Traps with NO2 + O2 and NO + O2: Effects of Pt, Ba loading, Catal. Today. 151 (2010) 291–303. https://doi.org/10.1016/j.cattod.2010.02.024.

[27] L. Castoldi, R. Matarrese, S. Morandi, L. Righini, L. Lietti, New insights on the adsorption, thermal decomposition and reduction of NO x over Pt- and Ba-based catalysts, Appl. Catal. B Environ. 224 (2018) 249–263. https://doi.org/10.1016/j.apcatb.2017.10.019.

[28] R.D. Clayton, M.P. Harold, V. Balakotaiah, C.Z. Wan, Pt dispersion effects during NOx storage and reduction on Pt/BaO/Al2O3 catalysts, Appl. Catal. B Environ. 90 (2009) 662–676. https://doi.org/10.1016/j.apcatb.2009.04.029.

[29] W.P. Partridge, J.S. Choi, NH3 formation and utilization in regeneration of Pt/Ba/Al2O3 NOx storage-reduction catalyst with H2, Appl. Catal. B Environ. 91 (2009) 144–151. https://doi.org/10.1016/j.apcatb.2009.05.017.

[30] S. Shwan, W. Partridge, J.S. Choi, L. Olsson, Kinetic modeling of NOx storage and reduction using spatially resolved MS measurements, Appl. Catal. B Environ. 147 (2014) 1028–1041. https://doi.org/10.1016/j.apcatb.2013.10.023.

[31] R.D. Clayton, M.P. Harold, V. Balakotaiah, NOx storage and reduction with H2 on Pt/BaO/Al2O3 monolith: Spatio-temporal resolution of product distribution, Appl. Catal. B Environ. 84 (2008) 616–630. https://doi.org/10.1016/J.APCATB.2008.05.018.

[32] J.S. Choi, W.P. Partridge, M.J. Lance, L.R. Walker, J.A. Pihl, T.J. Toops, C.E.A. Finney, C.S. Daw, Nature and spatial distribution of sulfur species in a sulfated barium-based commercial lean NOx trap catalyst, in: Catal. Today, 2010. https://doi.org/10.1016/j.cattod.2010.01.016.

[33] M. Maurer, T. Fortner, P. Holler, S. Zarl, H. Eichlseder, Impact of cyclic lean–rich aging under DeSO x condition on the lean-gas light-off and hydrogen formation ability of a lean NO x trap (LNT), Automot. Engine Technol. 2 (2017) 63–77. https://doi.org/10.1007/s41104-017-0019-3.

[34] P.R. Dasari, R. Muncrief, M.P. Harold, Elucidating NH 3 formation during NO x reduction by CO on Pt-BaO/Al 2O 3 in excess water, Catal. Today. 184 (2012) 43–53. https://doi.org/10.1016/j.cattod.2011.12.009.

[35] K. Hadl, R. Ratzberger, H. Eichlseder, M. Schuessler, W. Linares, H. Pucher, Sulfur Poisoning of a NO $_x$ Storage Catalyst - A Comprehensive Modelling Approach, SAE Int. J. Engines. 9 (2016) 2016-01–0964. https://doi.org/10.4271/2016-01-0964.

[36] M. Alain, M. Jacques, M.B. Diane, P. Karine, MAX: Multiplatform applications for XAFS, J. Phys. Conf. Ser. 190 (2009) 0–4. https://doi.org/10.1088/1742-6596/190/1/012034.

[37] M. Newville, EXAFS analysis using FEFF and FEFFIT, J. Synchrotron Radiat. 8 (2001) 96–100. https://doi.org/10.1107/S0909049500016290.

[38] C. Coney, C. Hardacre, K. Morgan, N. Artioli, A.P.E. York, P. Millington, A. Kolpin, A. Goguet, Investigation of the oxygen storage capacity behaviour of Three Way Catalysts using spatio-temporal analysis, Appl. Catal. B Environ. (2019). https://doi.org/10.1016/j.apcatb.2019.117918.

[39] Z. Say, E.I. Vovk, V.I. Bukhtiyarov, E. Ozensoy, Influence of ceria on the NOxreduction performance of NOxstorage reduction catalysts, Appl. Catal. B Environ. 142–143 (2013) 89–100. https://doi.org/10.1016/j.apcatb.2013.04.075.

[40] V. Marchionni, Modulated excitation and phase sensitive detection for the investigation of elementary catalytic reactions, Dr. Thesis. (2017). https://doi.org/https://doi.org/10.3929/ethz-b-000166278 Rights.

[41] A.K. Datye, Q. Xu, K.C. Kharas, J.M. McCarty, Particle size distributions in heterogeneous catalysts: What do they tell us about the sintering mechanism?, Catal. Today. 111 (2006) 59–67. https://doi.org/10.1016/j.cattod.2005.10.013.

[42] P.N. Plessow, F. Abild-Pedersen, Sintering of Pt Nanoparticles via Volatile PtO2:

Simulation and Comparison with Experiments, ACS Catal. 6 (2016) 7098–7108. https://doi.org/10.1021/acscatal.6b01646.

[43] T.R. Johns, R.S. Goeke, V. Ashbacher, P.C. Thüne, J.W. Niemantsverdriet, B. Kiefer, C.H. Kim, M.P. Balogh, A.K. Datye, Relating adatom emission to improved durability of Pt-Pd diesel oxidation catalysts, J. Catal. 328 (2015) 151–164. https://doi.org/10.1016/j.jcat.2015.03.016.

[44] Y. Ji, V. Easterling, U. Graham, C. Fisk, M. Crocker, J.S. Choi, Effect of aging on the NOx storage and regeneration characteristics of fully formulated lean NOx trap catalysts, Appl. Catal. B Environ. 103 (2011) 413–427. https://doi.org/10.1016/j.apcatb.2011.02.005.

[45] X. Auvray, L. Olsson, Stability and activity of Pd-, Pt- and Pd-Pt catalysts supported on alumina for NO oxidation, Appl. Catal. B Environ. 168–169 (2015) 342–352. https://doi.org/10.1016/j.apcatb.2014.12.035.

[46] V. Easterling, Y. Ji, M. Crocker, M. Dearth, R.W. McCabe, Application of spaciMS to the study of ammonia formation in lean NO x trap catalysts, Appl. Catal. B Environ. 123–124 (2012) 339–350. https://doi.org/10.1016/j.apcatb.2012.05.002.

[47] S.S. Mulla, S.S. Chaugule, A. Yezerets, N.W. Currier, W.N. Delgass, F.H. Ribeiro, Regeneration mechanism of Pt/BaO/Al2O3 lean NOx trap catalyst with H2, Catal. Today. 136 (2008) 136–145. https://doi.org/10.1016/j.cattod.2008.01.007.

[48] R.D. Clayton, M.P. Harold, V. Balakotaiah, NOx storage and reduction with H2 on Pt/BaO/Al2O3 monolith: Spatio-temporal resolution of product distribution, Appl. Catal. B Environ. (2008). https://doi.org/10.1016/j.apcatb.2008.05.018.

[49] A.M. Gänzler, M. Casapu, F. Maurer, H. Störmer, D. Gerthsen, G. Ferré, P. Vernoux, B. Bornmann, R. Frahm, V. Murzin, M. Nachtegaal, M. Votsmeier, J.D. Grunwaldt, Tuning the Pt/CeO2 Interface by in Situ Variation of the Pt Particle Size, ACS Catal. 8 (2018) 4800–4811. https://doi.org/10.1021/acscatal.8b00330.

[50] L. Lietti, I. Nova, P. Forzatti, Role of ammonia in the reduction by hydrogen of NOx stored over Pt-Ba/Al2O3 lean NOx trap catalysts, J. Catal. 257 (2008) 270–282. https://doi.org/10.1016/j.jcat.2008.05.005.

[51] L. Cumaranatunge, S.S. Mulla, A. Yezerets, N.W. Currier, W.N. Delgass, F.H. Ribeiro, Ammonia is a hydrogen carrier in the regeneration of Pt/BaO/Al2O3 NOx traps with H2, J. Catal. 246 (2007) 29–34. https://doi.org/10.1016/j.jcat.2006.11.008.